

Effect of Ambient Air Temperature on the Compression Wave Propagating along a Railway Tunnel

R. S. Iyer¹, D. H. Kim² and H. D. Kim^{1†}

¹ Department of Mechanical Engineering, Andong National University, Andong, Korea Republic

² Hypertube Express (HTX) Research Team, Korea Railroad Research Institute, Gyeonggi, Korea Republic

†Corresponding Author Email: kimhd@anu.ac.kr

(Received July 18, 2022; accepted January 24, 2023)

ABSTRACT

The parameters of the compression wave propagating in a railway tunnel are significantly influenced by the large ambient air temperature variation throughout the year. High-speed train entering a railway tunnel produces a wave of finite amplitude to propagate at sonic speed. The wave attenuates while propagation through viscous dissipation and inertial forces nonlinearly steepen the wave. As a result of the dependence of sound speed on air temperature, the wave characteristics are altered with changing temperature. Therefore, it is crucial to comprehend the impact of ambient air temperature on the properties of the compression wave in order to construct an aero-acoustically ideal railway tunnel system. The method of characteristics (MOC) has been used to solve Euler equations with steady and unsteady friction parameters in the current study. According to the findings, wave attenuation ratio is reducing along the tunnel length, and gradient is rising as train speed increases. The case study illustrates the key distance within a tunnel where the steepening ratio is at its highest point. This critical tunnel length is estimated to be 65 times the tunnel hydraulic diameter (300 km/h) for a particular air temperature ($T = 323$ K), and it decreases by 15% for a 70 K reduction (323K to 253K) in temperature. Similarly, the critical length falls by 40% for greater train speeds (500 km/h).

Keywords: Non-linear effect; Tunnel aeroacoustics; Unsteady friction; Wave distortion; Wave propagation.

NOMENCLATURE

A	cross-sectional area of train	T	static temperature
A_{tun}	cross-sectional area of tunnel	u	velocity
c	local speed of sound	U	train speed
D_h	tunnel hydraulic diameter	M_t	train Mach number
e	internal energy	W	weighting function
f_s	steady friction	γ	ratio of specific heat capacities
f_{us}	unsteady friction	ε_{us}	unsteady friction constant
km	kilometer	μ	dynamic viscosity of fluid
km/h	kilometer per hour	ν	kinematic viscosity of fluid
L	tunnel length	ρ	density
p	static pressure	τ	backward time or retarded time
R	gas constant	ϕ	train to tunnel blockage ratio, A/A_{tun}
t	time	ζ	wave attenuation ratio
Re_a	acoustic Reynolds number	ξ	wave steepening ratio

1. INTRODUCTION

High-speed trains act as a piston during tunnel ingress, thus generating a significant pressure disturbance that travels at local sonic velocity (c) (Yamamoto 1977). The wave gets distorted during the propagation process due to the losses occurring as a result of the wall skin friction and the inertial

forces along the tunnel length (Matsuo *et al.* 1996; Mashimo *et al.* 1997; Kim and Setoguchi 1999; Raghunathan *et al.* 2002; Fukuda *et al.* 2006). However, the wave velocity (c) is governed by the local air temperature (i.e., $c = \sqrt{\gamma RT}$). As a result, the distortion properties of the wave are significantly impacted by the considerable seasonal fluctuations in ambient air temperature (T). The reduction in the pressure magnitude over tunnel distance, pressure

gradient and wave thickness differ considerably with local air temperature. Moreover, with the advent of increasing train speed, having a tunnel design that strictly adheres to the noise standards set by government bodies has become extremely challenging. The increased concern with a train-tunnel system is the emission of high amplitude micro-pressure waves (MPWs) due to a steep wave reaching the tunnel exit. The emitted MPWs produce a loud tunnel boom that can cause severe rattling and vibration to nearby structures and buildings. In addition, given the variations in air temperature are considerably large in many countries (especially in South Korea), the chances of a steep wave manifesting due to seasonal changes is inadvertently quite high. Therefore, the average annual air temperature distribution in a tunnel has become an essential aspect to be considered. Furthermore, understanding the physics underlying wave mechanics at various air temperatures has also developed into a useful case study in the field of gas dynamics. The applications are not restricted to railroad tunnels, the elucidation of the flow physics can also be extended to numerous compressible flow problems.

The flow properties of the compression wave in railway tunnels continue to be of relevance to gas dynamists as well as tunnel researchers across the globe (Howe *et al.* 2000; Miyachi *et al.* 2008, 2016 a, b, 2017; Iyer *et al.* 2018, 2020, 2021; Heine *et al.* 2018; Kim *et al.* 2021). It has been adjudicated that the characteristics of the waves during propagation depend on the inertial forces, which lead to non-linear waveform distortion and tunnel wall friction (i.e., steady and unsteady) that initiate viscous dissipation. However, as field measurements (Jun *et al.* 2017; Zhao *et al.* 2020) from railway tunnels have reported substantial variation in air temperature ($\Delta T=70K$) during the course of the year, the propagation characteristics need to be corroborated for temperature effect as well. Air temperatures reach nearly 323K (50°C) during summers and drop gradually to a value of 253K (-20°C) in the wintertime. Railway tunnels in the Gangwon province of South Korea (Jun *et al.* 2017) and the Zuomutai tunnel (Zhao *et al.* 2020) in the northeastern part of China have registered average temperature variations in the range of 316K (43°C) to 248K (-25°C). These large air temperature variations can alter the wave characteristics as it propagates along tunnel, thereby emitting strong MPWs with significant magnitudes, even after pertinent countermeasures are installed in the tunnels. Thus, the authors were encouraged to conduct a thorough investigation that shed light on the impact of temperature variations of the ambient air over the flow properties of compression wave in railway tunnels.

In the last three decades, Japanese and German researchers have studied wave propagation characteristics extensively through field measurements (Matsuo *et al.* 1996; Mashimo *et al.* 1997; Fukuda *et al.* 2006; Adami and Kaltenbach 2008; Heine *et al.* 2018) and numerical analyses (Miyachi *et al.* 2016 a, b). The studies have helped

tunnel researchers (Mok and Yoo 2001; Howe *et al.* 2000; Winslow *et al.* 2005; Iida and Howe 2007; Murray and Howe 2010; Zhang *et al.* 2017; Kim *et al.* 2021) to develop state-of-the-art entrance hoods that have proven to be the best countermeasure for alleviating MPWs radiating from end of a tunnel. However, to ensure the effectiveness of hoods, especially with overlong tunnels, a thorough assessment of the propagation characteristics must be performed. The reason could be due to the changing wave characteristics during the propagation process. Thereby the wave near the exit of tunnel differs by a large extent from the one formed near the entrance. Therefore, this could lead to uncertainties in predicting steepness and magnitude of the wave inside tunnel and at exit. Thus, the intended purpose of the entrance hood has been rendered ineffective in such cases, thereby transmitting undesirable high amplitude MPWs from the tunnel exit. Perhaps the analyses before hood design can potentially be a more lucrative option. The main objective of the entrance hood is to alleviate the steepness of the wave generated near the entrance of the tunnel. Thus, designers need to resort to other options such as extending the train noses, reducing train speeds for a short period inside the tunnels, and creating a side window or side branch to take care of the subsequent wave steepening during propagation. The practices are effective to a certain extent in alleviating the wave steepness, but they add heavy costs to the existing hood design and are difficult to maintain. In practice, the compression wave characteristics under different air temperature conditions not only can provide designers a rapid assessment tool to develop state-of-the-art countermeasures (e.g., entry hoods, flared extensions, windows), but also to perceivably model the inline ventilation systems of railway tunnels.

Previous studies on the propagation process of compression waves have examined the effect of friction alone (Fukuda *et al.* 2006; Adami and Kaltenbach 2008; Miyachi *et al.* 2016a, b; Wang *et al.* 2018; Iyer *et al.* 2021). The studies have contributed immensely to tunnel research on the wave propagation mechanism, but they excluded the effect of air temperature variations. In addition to entry hoods, Li (2016) showed that providing side branches along the tunnel length can alleviate wave steepening during the propagation process. Nonetheless, the heavy construction costs incurred for both the side branches and tunnel hoods have made them an impractical and uneconomical solution. To the authors' best understanding and from the literature survey conducted, the most suitable option is to theoretically evaluate the changes occurring to wave properties under different ambient air temperatures before hood design. The analyses will offer a detailed insight into the underlying wave mechanism. In addition, the findings can be a key factor in deciding an aero-acoustically optimal solution to wave steepening problems in tunnels.

A train-tunnel system with the internal wave phenomena are schematically depicted in Fig. 1. The wave generated near the entrance travels inside the

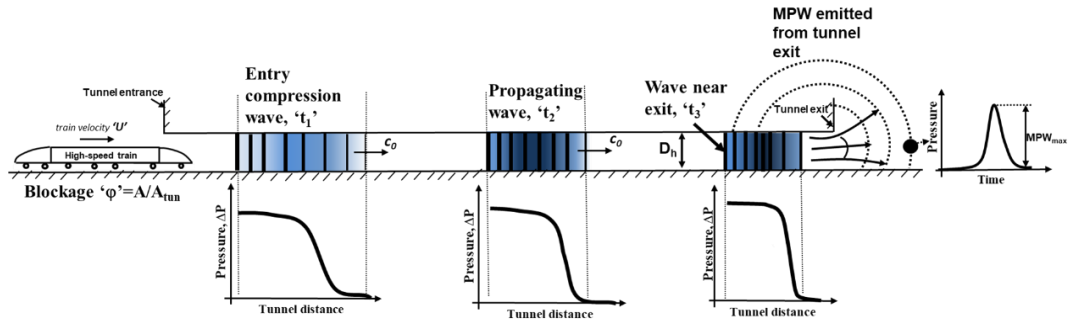


Fig. 1. Schematic for wave propagation mechanism in train-tunnel system.

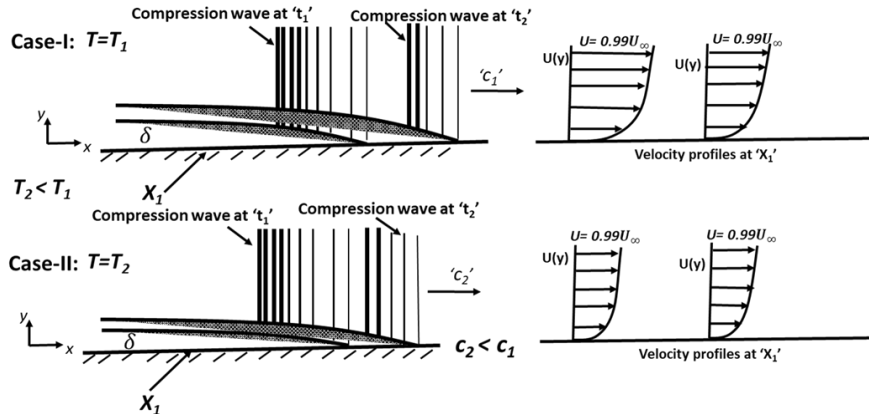


Fig. 2. Schematic of the velocity profiles at different ambient air temperatures inside tunnel.

tunnel and radiates from the end as a weak pulse (viz. MPW) causing a ‘tunnel boom’. The boundary layer created by the compression wave during propagation in a tunnel is presented by a detailed schematic in Fig. 2. The unsteady nature of the flow inside the tunnel causes the boundary layer created by the compression wave to change over time. The flow properties fluctuate as a result of this and due to the changing boundary layer attributes, the wave properties undergo significant change locally along the distance of tunnel. Additionally, consider the air temperature changes to “ T_2 ” (case-II), the compression wave velocity is altered (shown by ‘ c_2 ’) causing the wave properties to totally differ from case-I. Thereby, the induced boundary layer by the propagating compression wave also changes in comparison to case-I.

A frequency dependent friction model that takes into consideration the past flow record and compensates for the absence of extra damping during wave propagation is especially important for accurately predicting transient flows in tunnels. This damping may become even more significant in extremely long tunnels, resulting in a considerably quicker rate of wave distortion. The wave tends to change form faster than the one predicted with a constant frictional component. To anticipate the compression wave propagating through a railway tunnel, it is critical to consider frequency dependent friction component. Only accounting for the momentary resistance created toward the flow would disregard the higher harmonic components in the wave. It would calculate the flow properties moving through viscous dissipation, but only for the attenuation of

lower harmonic components. When compared to lower harmonic components, higher harmonic components distort or attenuate at a considerably quicker rate. The Darcy-Weisbach friction model can only estimate steady friction forces on the compression wave as it propagates. As a result, the unsteady friction model was incorporated in the present research for precise predictions. The method of characteristics (MOC) technique was implemented for solving the set of equations.

For continued relevance, the one-dimensional Euler equations were selected for the numerical analysis in the current study. The one-dimensional analysis with Euler equations that had friction source terms was the best choice, as they are computationally cost-effective as well as provide greater ease in understanding the behavioral changes of the flow properties. In recent studies, extensive applications of one dimensional analytical and numerical solutions have been suggested for interpreting flow physics. Amid many such studies were the solutions obtained using one dimensional analysis to predict interactions between a weak discontinuity with characteristic shock waves in compressible flows (Zeidan *et al.* 2021). Ouffa *et al.* (2021) expanded the investigations to two-phase gas-liquid compressible flows using drift-flux models. Furthermore, the studies have extended to applications of Aerogels (Zeidan *et al.* 2021) and using a one-dimensional numerical analysis for solving multiphase flow problems (Kozakevicius *et al.* 2018). Similarly, Zeidan *et al.* (2006) proposed a solution for the more complicated two-phase compressible flows using one dimensional analysis. It is thus quite fair to say

that most gas dynamic studies can be reasonably conducted in simplicity using the one-dimensional Euler equations. The wave mechanism studies undertaken lately have delivered results of colossal value to the gas dynamic community. However, the focus of the current research was essentially to examine the rate at which the properties of the wave change as it travels along railway tunnels, which were seldom dealt with in previous studies. Considering the research literature, the present study can be treated as novel, specifically in the area of tunnel aeroacoustics. The data provide an accurate evaluation of wave dynamics for a given tunnel length, as well as friction factors and a qualitative interpretation of the physics under different ambient air temperature conditions.

The work in this paper describes the wave dynamics during propagation along a straight railroad tunnel (for simplification, no inline vents, ducts, or track features were considered). The analysis was performed to understand the effect of four different air temperatures (viz., 253K, 273K, 300K and 323K) on the wave characteristics. As the aim of the current analyses is focused on concisely assessing the broad dependance of compression wave characteristics on temperature, the attention was then directed towards two extreme temperature scenarios (i.e., 253K and 323K). Later, the friction factors and train speed were varied at these two temperatures. The technical development of the numerical method begins in the following section (Section 2). Due to its robustness in obtaining precise solutions to hyperbolic partial differential equations, the method of characteristics (MOC) technique was chosen here to solve the set of governing equations (PDEs). Firstly, the results were compared with data obtained from a reduced model experimental setup. After establishing the base case, the influence of the a) air temperature (section 3.1), b) steady and unsteady friction (section 3.2), and c) train speed (section 3.3) were considered, leading to predictions of the critical tunnel length (section 3.4).

2. THEORETICAL ANALYSIS

2.1 Governing Equations

To simplify the analysis, wave propagation in straight tunnels can be approximated to a one-dimensional phenomenon. The flow features can be predicted with good accuracy using one-dimensional equations of continuity, momentum, and energy. Using the relation presented in equation 1, the wave profile and magnitude at the entrance is determined based on the train speed and blockage ratio (“ A/A_{tun} ”) (Hara 1961; Miyachi 2017) (“ M_t ” is Mach number (“ U/c ”) and “ φ ” blockage ratio).

$$\Delta P_{entry} = \frac{\gamma p M_t^2 [\varphi^2]}{[(1 - \varphi)^2 + (1 + \varphi^2)M_t - M_t^2]} \quad (1)$$

Once the initial conditions were obtained using Eq. (1), the equations that determine the wave propagation inside tunnels could be written as follows:

$$\frac{\partial U}{\partial t} + \frac{\partial F}{\partial x} = -S \quad (2)$$

where;

$$U = \begin{pmatrix} \rho \\ \rho u \\ e \end{pmatrix}; F = \begin{pmatrix} \rho u \\ p + \rho u^2 \\ (e + p)u \end{pmatrix}; S = f_s + f_{us} \quad (3)$$

The density and absolute pressure here are “ ρ ” and “ p ” respectively, while “ u ” denotes velocity in the x -direction. The friction terms “ f_s ” and “ f_{us} ” together contribute to the source parameter “ S ”. The friction parameters provide resistance to the flow and hence the negative sign. The ideal gas relation, as shown in Eq. (4), where “ R ” is the gas constant yields specific internal energy “ e ” from temperature “ T ”.

$$p = \rho RT \quad (4)$$

The steady friction in this study is expressed by the following relation:

$$f_s = \frac{\lambda \cdot \rho(u + c)^2}{2D_h} \quad (5)$$

The “ λ ” in Eq. (5) is the steady friction factor, “ D_h ” is the tunnel hydraulic diameter, and “ c ” represents the speed of sound. The friction parameter “ f_s ” is obtained from Darcy-Weisbach empirical relation widely used in the modelling of pipe flows (Vardy and Brown 1995, 2000; Vardy *et al.* 2009). However, the frequency dependent friction term “ f_{us} ” accounts for the cumulative effect of instantaneous accelerations over a relatively long period of time. Just as the steady friction factor “ f_s ” depends on velocity, the unsteady friction term depends on the rate of change of velocities. The current analyses necessitate recalling the unsteady friction term since velocity profiles across the tunnel respond to the changes occurring in the mean flow. Thus, there may be significant differences in the velocity profiles obtained from steady and unsteady frictions. It was therefore crucial to include unsteady friction in the current study to understand the characteristics of the wave, right from its initial stage of formation to propagation and until the end of the tunnel length. The form that Vardy and Brown (1995, 2000) and Vardy *et al.* (2009) developed for the frequency-dependent friction term has been extensively applied and accepted. In the current study the unsteady friction term “ f_{us} ” from Vardy and Brown (2000) was evoked once again (Eq. (6)):

$$f_{us} = \varepsilon_{us} \cdot \int_0^t W(\tau) \cdot \frac{\partial u}{\partial \tau} \cdot d\tau \quad (6)$$

The term “ ε_{us} ” denotes the unsteady friction factor, and “ $W(\tau)$ ” represents the weighting function that accounts for the previous changes in flow velocity over time. In view of the earlier work on wave propagation under frictional effects conducted by the authors (Iyer *et al.* 2021), the current investigation intended to pursue a similar direction. However, the

air temperature variation was also considered here. For a ready reference, the discretized form of the unsteady friction model is presented below in Eq. (7). The coefficients “ n_i ” and “ m_i ” change with distance and time, respectively, “ ϑ ” kinematic viscosity of the fluid, and “ D_h ” represents the tunnel hydraulic diameter. The weighting function “ $W(t)$ ” is formulated using Eq. (8), where the Reynolds number provides the value of “ B ” while dimensionless time “ ψ ” is deduced from hydraulic diameter “ D_h ” of tunnel. The weighting function asymptotically reduces with time, indicating lower weights as the wave propagates further downstream from the tunnel.

$$f_{us}(t + \Delta t) = \frac{16\vartheta}{D_h^2} \sum_{i=1}^N W(t) e^{-\left(\frac{4n_i\vartheta}{D_h^2}\right)} + \frac{m_i D^2}{4n_i\vartheta} \left(1 - e^{-\left(\frac{4n_i\vartheta}{D_h^2}\right)} \frac{\partial u}{\partial t} \right) \quad (7)$$

$$W(t) = \frac{1}{2\sqrt{\pi}\psi} e^{-B\psi} \quad (8)$$

2.2 Method of Characteristics

The method of characteristics (MOC) is an effective tool in practical applications that can provide superior prediction accuracies with great simplicity in solving. The study undertaken here used governing equations, which were hyperbolic partial differential equations (Eq. 9 to Eq. 11) that could not be integrated directly. Therefore, the equations needed to be cast into characteristic forms for ease of numerical simulation. The equations were written in such a manner so that they were valid in the “ $x-t$ ” plane, allowing them to be numerically solved in a regularly spaced grid. The set of equations (Eq. 12) were called the characteristic equations and were typical to MOC (Vardy and Brown 1995, 2000) The grid intervals were chosen internally based on the aero-acoustic theory that changed with density and temperature of the fluid and satisfied the characteristic direction presented in Eq. (13). The grid was updated instinctively so as to accommodate the convective velocity changes of the compression wave. This minimized numerical errors and prevented misinterpretation of the wavefront characteristics.

At all grid points in the tunnel, the wavefront adjusts itself to satisfy the criteria of the speed of sound equation (Eq. (14)) stated in terms of the square root of temperature. To numerically solve the set of equations, the accuracy was confined to the second order upwind scheme along with explicit Runge Kutta method for space and time respectively. The scheme has been previously shown to provide reasonable results on the qualitative end (Vardy and Brown 1995, 2000; Iyer *et al.* 2021) and the completeness of the quantitative origins was also

reviewed. The governing equations are solved using the second-order finite difference approach with Roe's approximation. The value of the entry wave for a given ambient air temperature (T) and the local sound speed were used to define the initial condition for the computational analyses. The boundary conditions downstream of the computational domain were maintained constant while the propagation of the compression wave and the pressure value upstream were the only factors contributing variations that occurred later inside the tunnel. The tunnel wall was considered adiabatic, as it had significant thickness that could have negligible interactions from outside air and little effect on the ambient air temperature inside them. Therefore, the wall temperatures were considered to be constant and assumed to be at T=300K.

The current study involves a straight long tunnel without any area variations, ventilation shafts, windows, branches and track features such as ballast and slab. Only the generated wave by the train is considered which is derived directly from Eq. (1). Afterward, the propagation of the wave is examined under different temperatures and friction conditions. The simulation started with an initial air density of 1.0kg/m³ and value of Courant number as 1. The value of universal gas constant “R” here is 287Jkg⁻¹K⁻¹ and 1.4 for the ratio of specific heats “ γ ” (air ideal gas). For convenience, the simulations were conducted using ideal gas equation of state (EOS).

The simulation began with a waveform that propagated in time with initial conditions inside the tunnel as described earlier. The tunnel geometry was discretized into equidistant grid points based on the “ Δx ” value obtained from Eq. (17) and Eq. (18). Based on the convective velocities (“ $U+C$ ”), the time step “ Δt ” was decided, which was then used to calculate the grid distance “ Δx ”. The air temperature variation was incorporated into the equation of state (EOS) (Eq. (4)), which was coupled with the energy and momentum equations (Eqs. 10 and 11). As the speed of sound varied with air temperature, the characteristic grid was updated along with the system of equations, as shown in Eqs. (15-18). The equations used for the current analyses are summarized below.

Continuity:

$$\frac{\partial \rho}{\partial t} + \rho \frac{\partial u}{\partial x} + u \frac{\partial \rho}{\partial x} = 0 \quad (9)$$

x-Momentum:

$$\rho \frac{\partial u}{\partial t} + u \frac{\partial \rho}{\partial t} + \frac{\partial p}{\partial x} + 2\rho u \frac{\partial u}{\partial x} = -f_{total} \quad (10)$$

Energy:

$$\frac{\partial e}{\partial t} + e \frac{\partial u}{\partial x} + u \frac{\partial p}{\partial x} + p \frac{\partial u}{\partial x} = 0 \quad (11)$$

Eqs. 9-11 were then cast into characteristic forms and their direction was written as follows:

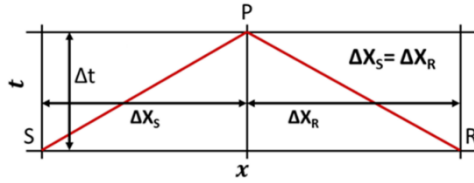


Fig. 3. Characteristics grid lines used for the method of characteristics (MOC) analysis.

$$\frac{2}{\gamma - 1} \frac{dc}{dt} \pm \frac{\partial U}{\partial t} = \mp f_{total} \quad (12)$$

Eq. (12) is valid in the space-time ($x-t$) as follows:

$$\frac{dx}{dt} = U \pm c \quad (13)$$

The propagating speed of the compression wave “ c ” was related to the ambient air temperature by Eq. (14):

$$c_1 = \sqrt{\gamma RT_1} \quad (14)$$

Where “ T_1 ” is the initial ambient air temperature.

The characteristics, left and right running were obtained from Eq. (12) and Eq. (13) on a grid (say, “S” and “R” are fixed grid points and “P” is based on the value of the time interval “ Δt ”; see Fig. (3)).

$$\frac{2}{\gamma - 1} (c_P - c_S) + (U_P - U_S) = -f_{total} \quad (15)$$

$$\frac{2}{\gamma - 1} (c_P - c_R) - (U_P - U_R) = f_{total} \quad (16)$$

$$(x_P - x_S) = (U_S - c_S)(t_P - t_S) \quad (17)$$

$$(x_P - x_R) = (U_R + c_R)(t_P - t_R) \quad (18)$$

$$f_{total} = f_s + f_{us} \quad (19)$$

In the equations presented above, the “ f_{total} ” is the total friction expressed as a sum of steady friction “ f_s ” and unsteady friction “ f_{us} ” (Eq. (19)). Hence, it would be quite right to say the character of the solution depends on the right-hand side (RHS) of the equation.

2.3 Validation and Verification

The accuracy of the numerical methodology was confirmed by validating alongside the data obtained from an experiment conducted on a model test rig (Kim *et al.* 2021). However, in order to assess the theoretical methodology, it is necessary to have meaningful comparisons with pressure histories obtained from an existing real railway tunnel. The comparisons of such a type have been previously

obtained and verified by the authors against a Japanese Shinkansen tunnel (Iyer *et al.* 2021). Based on the agreement with the real-time data, the numerical scheme was used for the current study.

Furthermore, for practical purposes and reconfirmation of the numerical methodology, the values obtained from the numerical simulation were re-verified once again against the experimental data. A 1/63rd reduced scale experimental setup of a real tunnel has been designed at the Korea Railroad Research Institute (KRRRI). The train model can be accelerated up to a constant speed of 350km/h along a steel guided wire throughout the length of the tunnel. The detailed descriptions of the experimental setup, complete guide on the tunnel model's measurements and the placements of the pressure sensors are documented in detail in Kim *et al.* (2021). The readers are encouraged to refer Kim *et al.* (2021) for extensive particulars on the experimental investigation and test conditions involved in obtaining the particular data, as the discussion falls beyond the scope of this paper.

The comparison of the pressure histories at various locations from KRRRI model and data predictions produced from numerical simulations is shown in Fig. 4. For the condition of steady friction factor “ λ ” which has a value of 0.5, and unsteady friction factor “ ϵ_{us} ” value of 10, the pressure histories of the two cases are in good agreement.

The numerical simulations included the tunnel geometry where in an entry compression wave generated for a train speed of 300km/h and a blockage ratio “ ϕ ” of 0.2 propagates at local speed of sound. The entry compression wave was generated to be similar to that of the experimental test rig conditions, which resembled the ones taken up in numerical simulations.

Thereafter, the changes that occurred were a consequence of the solved governing equations with source terms along the tunnel length. Although from Fig. 4 the numerical results show a small dispersion, the overall form of the wave and peak magnitude agreed well with the experimental data for the steady and unsteady friction factors chosen (i.e., 0.5 and 10). For practical reasons, the qualitative agreement of the data was given more prominence compared to the quantitative ones. However, it was ensured that the data were checked for both measures equally with caution and confirmed to have shown no persistent errors in time. The friction factor values were selected based on previously conducted tunnel studies in Japanese Shinkansen lines (Matsuo *et al.* 1996; Fukuda *et al.* 2007; Miyachi *et al.* 2008; 2016a,b). Based on several measurements, the suggested range for the unsteady friction factor was between $1 < \epsilon_{us} < 20$. However, after a few careful evaluations, the value of the steady friction factor “ λ ” and unsteady friction factor “ ϵ_{us} ” of 0.5 and 10, respectively, showed sufficient agreement with the experimental data. Therefore, for the convenience of further analyses, the friction factor values of steady and unsteady were considered to be 0.5 and 10, respectively. Nevertheless, the individual effect of

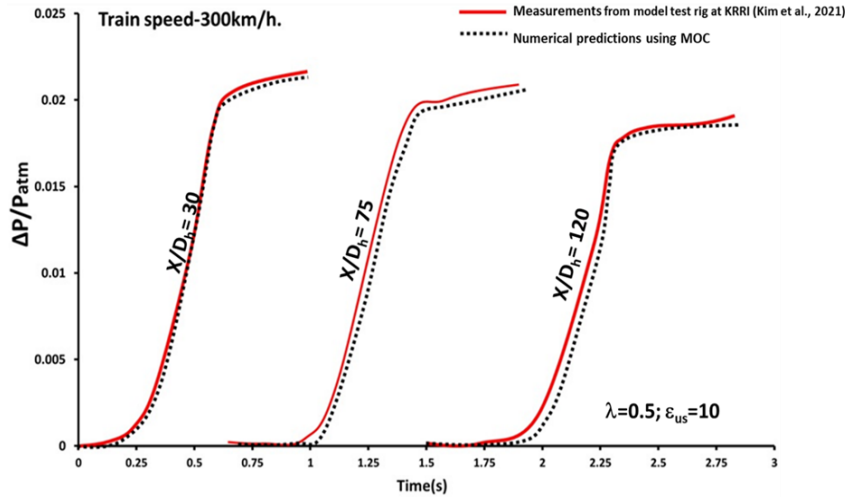


Fig. 4. Validation of numerical results with experimental data obtained from Model test at KRRI.

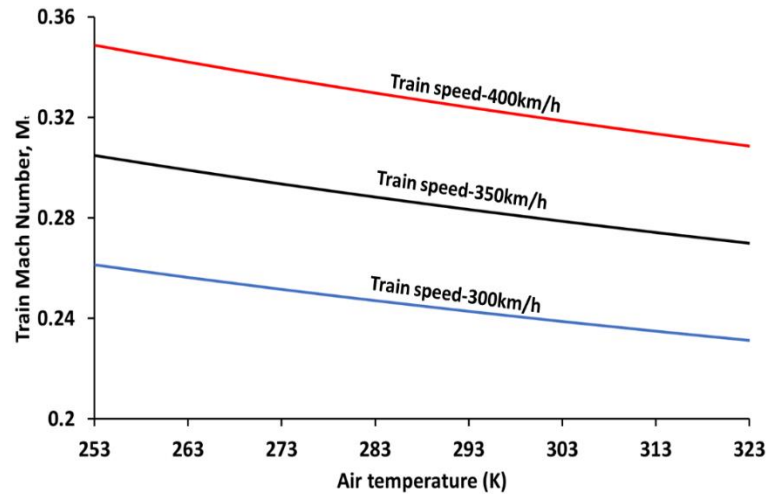


Fig. 5. Variation of train Mach number for different air temperatures at train entry speeds of 300km/h, 350km/h. and 400km/h.

the friction factors is taken up in following section for detailed discussion.

3. RESULTS AND DISCUSSION

3.1 Effect of Air Temperature

The quantification of the wave distortion in tunnels can be ascertained by the changes observed in the local values in the tunnel length. The ratio of corresponding local pressure to corresponding entry value at the tunnel section can provide a measure of linear distortion experienced by the wave. The peak over pressures at the entrance and local distance “ x ” can be written as “ $\Delta P(O)$ ” and “ $\Delta P(x)$ ”, respectively. Therefore, the attenuation ratio (i.e., linear distortion) presented by “ ζ ” becomes:

$$\zeta = \frac{\Delta P(x)}{\Delta P(O)} \quad (20)$$

Similarly, the variations in the maximum value of the steepness of the wavefront can be used to calculate the nonlinear distortion of the compression wave. The corresponding ratios of the maximum value of the steepness at a distance “ x ” from the entrance ($\frac{\partial p}{\partial t}|_{max,x}$) to the one found at the entrance section ($\frac{\partial p}{\partial t}|_{max,O}$) make up the steepening ratio “ ξ ”, which is represented below (Eq. (21)):

$$\xi = \frac{\frac{\partial p}{\partial t}|_{max,x}}{\frac{\partial p}{\partial t}|_{max,O}} \quad (21)$$

Since compression waves propagate with a fixed wavelength at a local speed of sound, temperature variation has a substantial effect on the propagation speed. Therefore, the train Mach number (“ M_i ”) can vary with the air temperature, as shown in Fig. 5. The trend observed is very essential to understand the

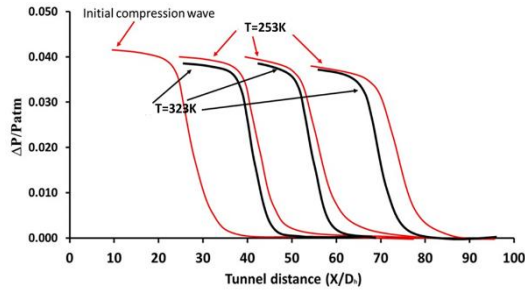


Fig. 6. Effect of the ambient air temperature on the compression wave propagating along a tunnel (T=253K and T=323K).

effect of temperature on wave propagation. From Fig. 5 it is noted that the train Mach number (“ M_t ”) decreases as the air temperature gradually increases from 253K to 323K. Here, the train Mach number is a ratio of the entry speed of train (U) to the local speed of sound (c). Therefore, this makes it an apt choice for depicting the average variations in wave propagation with temperature. A seemingly apparent consequence is the temperature increase causes the propagation speed to increase while the train speed entering the tunnel remains constant. When the train enters at a speed of 350km/h (shown by black line in Fig. 5), the train’s Mach number is seen to be dropping from a value of 0.3 to almost 0.27 by increasing the temperature from 253K to 323K. Thus, even though the train speed remains constant, the wave propagation speed (which is dependent on the local speed of sound, c) changes with the air temperature, ultimately affecting the train’s Mach number (“ M_t ”). Therefore, the evident result is: i) Changes in the peak pressure value of compression wave entering the tunnel given by Eq. (1) (ΔP_{entry} is a function of the train’s Mach number (“ M_t ”), and ii) As speed of sound is a function of temperature ($c = \sqrt{\gamma RT}$), the propagation speed of the wave adjusts accordingly for the length of the tunnel. Both these effects play a combined role in modifying the features of the wave during propagation.

Furthermore, to quantitatively demonstrate the effect of air temperature on compression wave propagation,

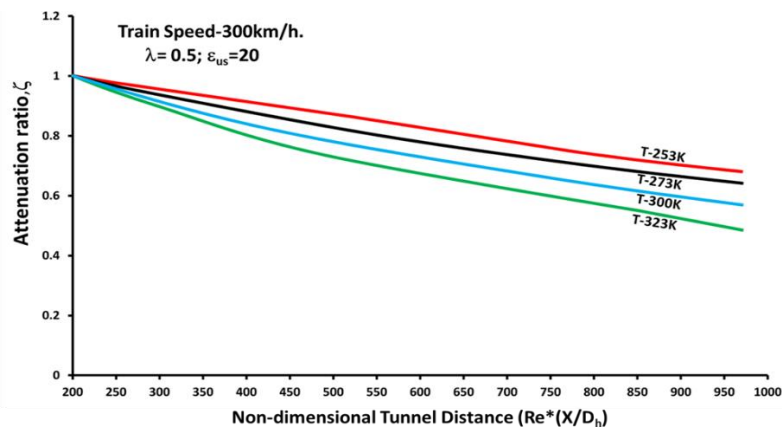


Fig. 7. Effect of ambient air temperature on the attenuation ratio of compression wave propagating along a tunnel ($\lambda=0.5$; $\epsilon_{us}=20$).

the pressure histories obtained from the monitors on the tunnel wall are plotted in Fig. 6 for the cases of 253K and 323K. As can be seen, the compression wave peak over pressure reduced noticeably for the case of 323K compared to the 253K temperature case. The results prove that temperature variation can change the density of the air and, subsequently, the peak over pressures largely differs for the two cases. An obvious reason is the higher temperature fluid being less dense compared to the fluid present at lower temperatures (e.g., 323K and 253K). However, the air at a higher ambient temperature propagates faster locally compared to lower temperature cases. This eventually affects the waveform and steepness of the compression wave, as the inertial forces are comparably higher for the lower temperature cases (i.e., 253K). Given a tunnel with long distances, which allows the propagation time to be infinite values, the waveform can undergo a non-linear effect, thus causing a steep wave to reach the exit portal. More precisely, the non-linear distortion that occurs in the wavefront when temperatures are lower (253K) is appreciably large enough to be compared with higher temperature cases (323K).

Figure 7 shows the attenuation ratio plotted against the non-dimensional tunnel distance ($Re^*(X/D_h)$) for ambient air temperature values of 253K, 273K, 300K, and 323K with a friction factor value of “ λ ” as 0.5 and an unsteady friction factor “ ϵ_{us} ” value of 20. The attenuation ratio becomes higher as the air temperature inside the tunnel increases. It is the lowest for the 253K case and the highest for the 323K case. In order to further clarify the effect of air temperature on the compression wave characteristics, the steepening ratio is plotted in Fig. 8 against the non-dimensional tunnel distance.

The steepening ratio is shown to be increasing as the temperature decreases. For the case of 253K, the steepening ratio reached a value of almost twice that of the initial compression waveform vicinity of tunnel end ($Re^*(X/D_h) = 900$). Therefore, a clear change in the distortion characteristics can be substantiated due to the difference in temperature ($\Delta T = 70K$).

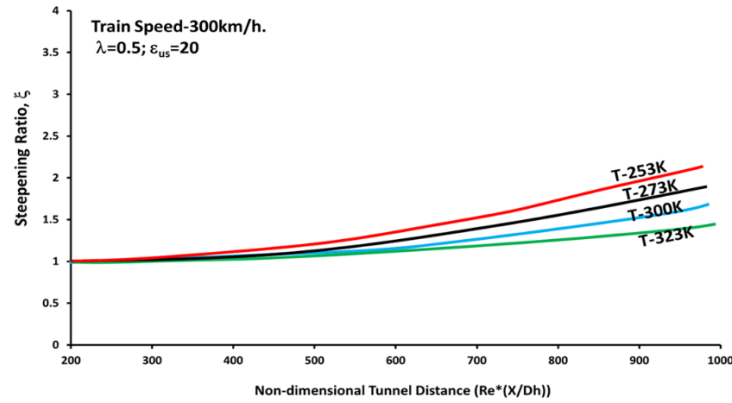


Fig. 8. Effect of ambient air temperature on the steepening ratio of the compression wave propagating along a tunnel ($\lambda=0.5$; $\epsilon_{us}=20$).

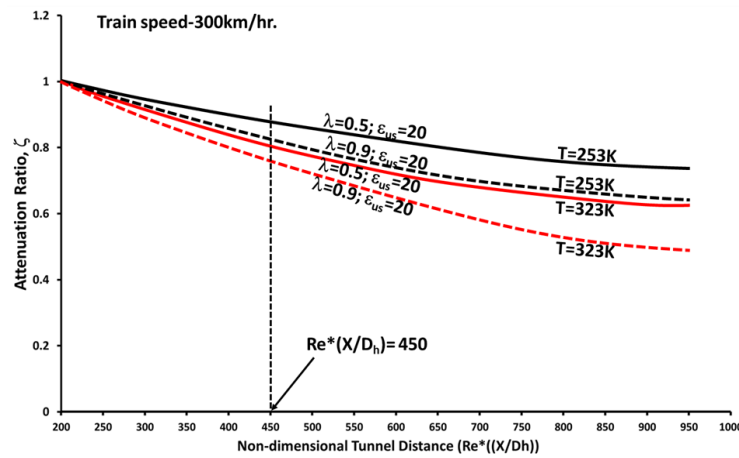


Fig. 9. Effect of steady friction factor on the attenuation ratio of compression wave propagating along tunnel ($T=253\text{k}$ and $T=323\text{K}$).

3.2 Effect of Steady and Unsteady Friction

Typically, the ratio of the dissipation component to the non-linear component for a propagating compression wave is expressed by the acoustic Reynolds number (Re_a). In this scenario, it would be correct to assert that the inertial forces and dissipation forces are equal at the threshold value (critical point) of the acoustic Reynolds number " Re^* ." nature of the waveform is influenced by the predominance of one distortion type over the other. When non-linear effects outweigh viscous effects, the waveform becomes steeper as it travels farther. On the other hand, if the viscous dissipation is larger, the wave begins to diminish over time as the distance increases. As a result, the wave steepening ratio becomes a crucial factor in determining the acoustic Reynolds number's threshold value. The steepening ratio mentioned by Eq. (21) increases exponentially as the tunnel distance increases. Hence, the criterion to obtain the critical Reynolds number is at the point where the steepening ratio becomes unity. At this location in the tunnel, both the viscous and inertial forces balance each other. The acoustic Reynolds number is as shown in Eq. (23) (" k " being the wave number). The criterion to obtain threshold of the acoustic Reynolds number is presented in Eq. (24). However, the value of the criterion becomes unity

when the constant " α " becomes zero (Eq. (25)). Furthermore, the criterion becomes greater than one when the " α " values are greater than one, thus indicating wave steepening, and the opposite holds true for " α " values lesser than one. Here, the critical acoustic Reynolds number was found to be approximately 120, and the subsequent non-dimensional tunnel distance, irrespective of all friction factor values, was found to be 450 ($Re^*(X/D_h)$).

$$Re^* = \frac{\pi(\gamma + 1)u_1 D_h}{2kc_1 L} \quad (23)$$

The criterion for obtaining the above Equation (Eq. (23)) is as follows:

$$\xi = e^{\left(\frac{\alpha X}{D_h}\right)} \quad (24)$$

$$\xi = 1 \quad (25)$$

Figure 9 shows the impact of the steady friction factor (λ) over the peak magnitude of propagating wave.

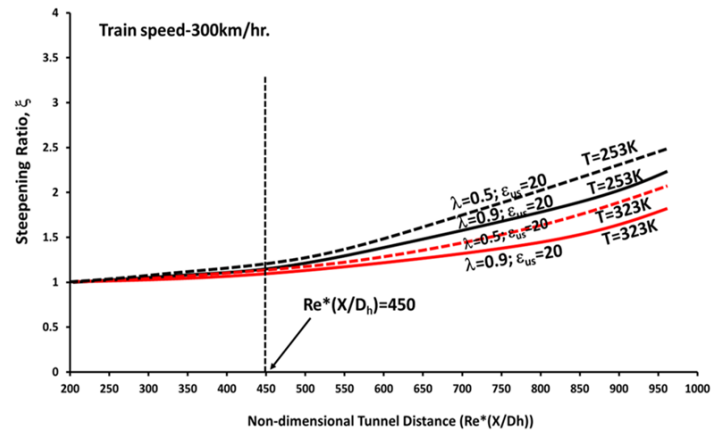


Fig. 10. Effect of steady friction factor on the steepening ratio of compression wave propagating along tunnel (T=253k and T=323K).

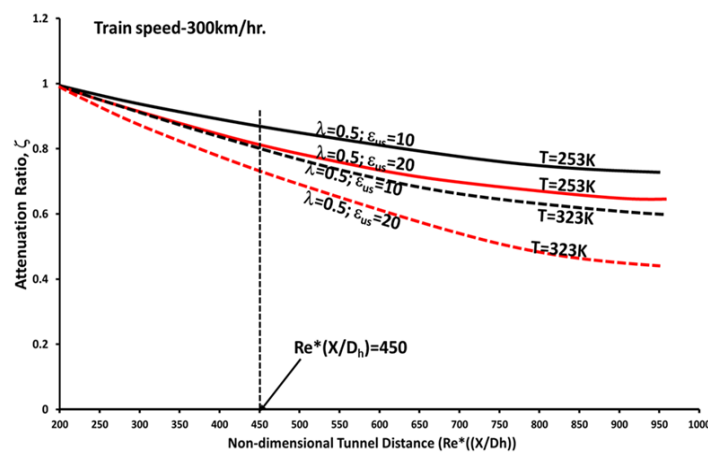


Fig. 11. Effect of unsteady friction factor on the attenuation ratio of compression wave propagating along tunnel (T=253k and T=323K).

The attenuation ratio indicates the peak over pressure amplitude changes for the two temperature cases tried here (253K and 323K). The attenuation ratio reduced more quickly for the higher temperature case of 323K. Furthermore, Fig. 10 depicts the rate of change of pressure gradient of the wave along the tunnel length for 253K and 323K air temperature cases when the steady friction factor changed from a value of 0.5 to 0.9. Figure 10 shows the effect of increasing steady friction factor from 0.5 to 0.9 at temperatures 253K and 323K. The gradient of the wave decreases along tunnel at the higher temperature (323K). Thereafter, when the air steady friction factor increases, the slope is seen to be decreasing further, showing a drop in the steepening ratios along the tunnel length, as shown in Fig. 10.

The influence of unsteady friction factor “ ϵ_{us} ” on the wave attenuation ratio “ ζ ” is depicted in Fig. 11. After meticulous validation, the values of the steady friction factor and the unsteady friction factor were chosen. The range of values was derived from actual tunnel investigations on German and Japanese tunnels. In this instance (Fig. 11), as unsteady friction factor increased from a value of 10 to 20 an accompanying shift in wave amplitude was noticed. The unsteady friction provided significant damping to the wave by offering cumulative resistance to the flow over the entire period of time

by means of the weighting function. Therefore, an obvious outcome for increasing the unsteady friction factor value from 10 to 20 would be greater attenuation and an additional drop in peak amplitude of the wave. However, the rate of change of the attenuation ratio along the tunnel length was different for the two air temperature scenarios.

To clearly depict the effect of temperature, the attenuation ratio was plotted for the case of 253K in the same plot. For the lower temperature case of 253K, the rate at which the attenuation ratio dropped was comparatively lower when compared to the 323K case. Consider the case of 323K and the unsteady friction factor value 10 (black dashed line in Fig. 11), the attenuation ratio reached a value of 0.7 near the tunnel exit (30% reduction in peak over pressure), whereas, for the same unsteady friction factor value of 10 and the case of 253K (black solid line in Fig. 11) the attenuation ratio dropped to 0.8 near the tunnel exit (20% reduction in peak over pressure). In addition, when observing the difference in both temperature scenarios while increasing the frequency dependent friction factor value from 10 to 20 (red solid and dashed lines in Fig. 11), the rates were totally different. For the higher temperature case of 323K, the drop was found to be much higher when compared to 253K.

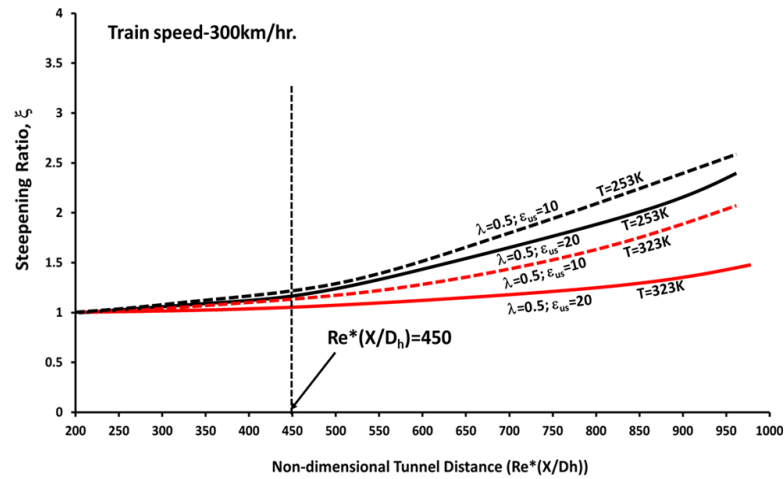


Fig. 12. Effect of unsteady friction factor on the steepening ratio of compression wave propagating along tunnel (T=253K and T=323K).

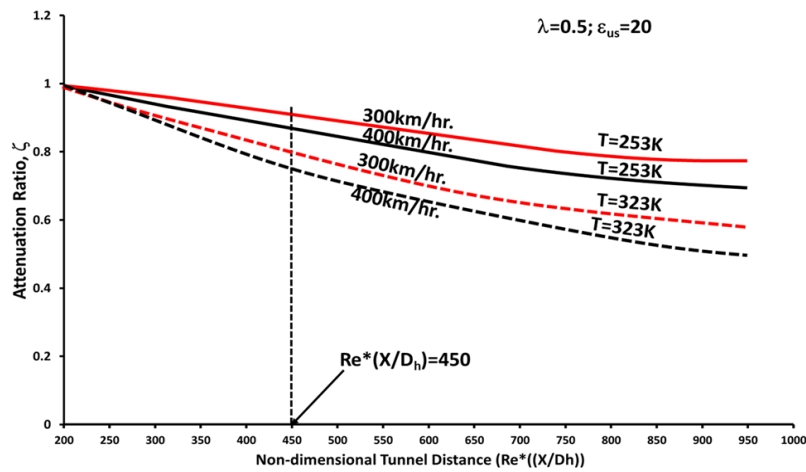


Fig. 13. Effect of train speed on the attenuation ratio of compression wave propagating along tunnel (T=253K and T=323K).

It follows that changes in air temperature have a significant impact on both the attenuation ratio of the compression wave and the rate at which attenuation ratios vary.

Figure 12 shows the effect of the frequency dependent friction factor on the waveform steepening plotted against the non-dimensional tunnel distance. As the temperature became lower, the waveform steepening became lesser. Although the rise in the unsteady friction factor produced a drastic reduction in the waveform steepness, with a higher temperature case of 323K, the wave was further flattened as it propagated along the tunnel. This could be attributed to the reduction in density as the temperature increased inside the tunnel. Heavier air (air at T=253K) could substantially give rise to higher inertial forces when compared to less dense air (air at T=323K). Thus, the curve can be seen as less steep for the higher temperature case of T=323K.

To encapsulate the results thus far, it is evident that the air temperature variations not only can affect the distortion characteristics significantly during wave propagation, but also the rates at which they change have been substantiated with quantitative data.

3.3 Effect of Train Speed

From a theoretical standpoint, the impact of train speed on the propagation phenomena was evaluated in order to predict compression wave characteristics. To simplify comparisons, the train speeds of 300km/h and 400km/h were used for the current study. For train speed 300km/h, a compression wave of finite wavelength (i.e., 35-50 times tunnel hydraulic diameter) and a peak over pressure of 3~4kPa above the atmospheric pressure were generated in a tunnel with blockage ratio (A/A_{tun}) of 0.2. In most countries with extremely long tunnels (approx. 7000~9000m), the trains travelling at such speeds (300~400km/h) transmitted MPWs of a magnitude 100~120Pa (approx. 130~140dBs) from the exit, which are detrimental in most environments. Hence, to comprehend the effect of train speeds at different air temperatures, the current analyses were simplified to a comparison of two cases, viz., 300km/h and 400km/h.

The wave attenuation and steepening ratio of the compression wave for both train speeds (300 km/h and 400 km/h) at 253 K and 323 K are shown in Figs. 13 and 14. According to the results, the 400 km/h

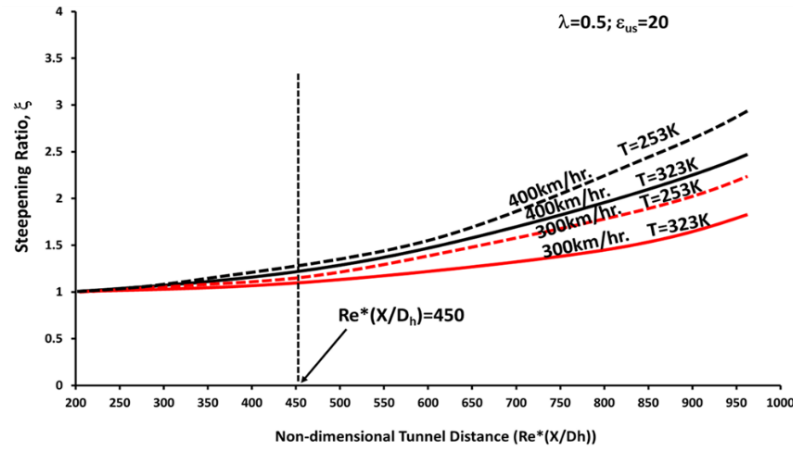


Fig. 14. Effect of train speed on the steepening ratio of compression wave propagating along tunnel (T=253K and T=323K).

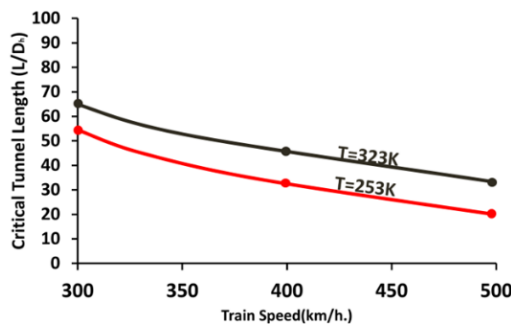


Fig. 15. Variation of critical tunnel length with train speed at different ambient air temperatures.

instance had a lower attenuation ratio for the compression wave than the 300 km/h train speed case. This indicates that a train traveling at a higher speed attenuated more quickly along the tunnel distance, with the attenuation ratio nearing 0.7 toward the end of the tunnel ($Re^*(X/D_h) = 900$) (see black solid line in Fig. 13) for 400km/h compared to 0.82 for the train traveling at a speed of 300 km/h (red solid line). This finding suggests that as train speed increases, viscous dissipation tend to be higher, resulting in a greater attenuation ratio reduction. However, with an increase in the ambient air temperature, the 323K case was considered for both speeds (red and black dashed lines in Fig. 13), the attenuation was much more enhanced (even more for 400km/h compared to 300km/h). The higher air temperature caused the compression wave to dissipate at a faster rate since the temperature change had a pronounced effect on viscosity, thereby leading to a greater drop in the attenuation ratio along the tunnel length (since viscosity and molecular action increased with temperature in compressible flows).

Now, drawing attention to the steepening ratio in Fig. 14, it could be seen that the steepening ratio increases from the non-dimensional tunnel distance ($Re^*(X/D_h)$) of 450, as the inertial forces dominated over the viscous forces beyond the critical Reynolds number (Re^*) of 120. This indicates the inception point in the tunnel, irrespective of the friction factor

values, and they were obtained as per the criteria defined in Eq. (23). However, due to the presence of the friction terms, the pressure gradient reached up to a value of 3 times initial value close to tunnel exit for the highest train speed case tried (400km/h, see black dashed line in Fig. 14). Hypothetically speaking, if the tunnel was assumed to be frictionless (inviscid), the gradient exponentially rose. In extremely overlong tunnels, where the propagation time tended to infinity, there was a discontinuity, or a shock wave observed in the flow. Nonetheless, in practical terms, such a sight has been extremely rare to observe in railway tunnels since there was sufficient viscous damping and the steepening ratio reached a maximum value of 3-3.5 (whereas the shock wave required at least 20~30). For the case of higher ambient air temperature (323K, red and black solid lines in Fig. 14), the steepening ratio decreased equally when compared to the 253K case for both train speeds of 300 and 400km/h.

3.4 Critical Tunnel Length

To recap, the influence of the blockage ratio and train speed on wave propagation under frictional effects was illustrated. Finally, a critical tunnel length was illustrated. Finally, a critical tunnel length must be determined for various train speeds in order to achieve a balance between the frictional forces and the viscous forces. The wave distortion achieves its greatest value at critical tunnel length (L/D_h), and when the tunnel length reaches this critical length, the inception point is achieved. Beyond this point in tunnel the strength of the compression wave intensifies and a steep wave with a high intensity reaches the tunnel exit, thereby leading to high amplitude MPW emissions.

Figure 15 represents the critical length of tunnel for distinct train speeds. The critical tunnel length for the case of 300 km/h is shown to have a value of 65 times the tunnel hydraulic diameter. As the train speed is raised to 500 km/h, the length decreases by approximately 45% (35 times the hydraulic diameter). Therefore, a train travelling at a speed 300km/h can cause the wavefront to steepen if the tunnel distances are greater than 65 times the

hydraulic diameter. Considering an identical tunnel cross-section and frictional parameters, a train travelling at 500km/h can cause the waveform to steepen at nearly a distance of 35 times the tunnel hydraulic diameter. Thus, higher train speeds tend to cause steepening at a much earlier stage inside the tunnel at lower ambient air temperatures. This holds true only for an ambient air temperature of 323K. Furthermore, if the lower temperature case of 253K is considered, the tunnel hydraulic diameter reduces by a value of 10 L/Dh compared to the higher temperature case. Overall, the critical length decreased virtually 15% compared to the 353K case. For a given tunnel and train speed, the critical tunnel length decreases for lower temperatures. The trend continues to remain the same as the train speed is further increased for the ambient air temperature of 253K. However, at a higher train speed, i.e., 500Km/h, the wave steepens at almost down to 20 times the hydraulic diameter for a lower ambient air temperature case of 253K. Hence, there is a 40% drop in the value of the critical length value for a drop of 70K in the ambient air temperature.

4. Conclusion

Here, numerical analysis was used to examine the compression wave properties as they propagated inside tunnels at various ambient air temperatures. The following points summarize the main findings of this investigation:

- (a) For particularly lower ambient air temperature cases ($T=253K$), the attenuation ratio and steepening ratio of the propagating wave were found to be considerably higher in comparison to the other case (323K).
- (b) As the friction factor was varied from $\lambda=0.5$ to 0.9 at 253K, the wave attenuation rate increased during propagation along the tunnel. An increment in ambient air temperature by 70K (323K) reduced the wave attenuation rate by 15%.
- (c) The waveform steepening ratio grew exponentially as the train speeds increased (almost cube of train speed). However, as the ambient air temperature increased from 253K to 323K, the growth became more gradual along the tunnel distance.
- (d) Finally, the trend of the critical tunnel length obtained here was observed as reducing with a rise in train speed. The quantitative values largely varied as the temperature decreased(253K). The critical length reduced by 15% at a train speed of 300 km/h and 40% with an increment in train speed by 200km/h.

In general, the results showed significant impact on the properties of the compression wave due to variations in the ambient air temperature. The analysis provides tunnel designers with a rapid evaluation of the allowable upper limit of train speed for a given tunnel of particular length, friction factor, and range of ambient air temperature variation throughout the year. Broadly speaking, conducting

meteorological surveys could provide an optimized design of tunnel countermeasures and ventilation systems. The final outcome suggests that the variations in the ambient air temperature greater than a value of 35K to 40K can largely affect the characteristics of the propagating wave. In the future, the authors intend to apply the current model for continuing studies that can further broaden and understand the wave mechanism in much more complex cases such as tunnels with air vents, shafts, openings, and hoods for a complete evaluation.

ACKNOWLEDGEMENTS

This research was supported by a grant from R&D program (Practical application of shark hood in conjunction with tunnel inner structures for reducing tunnel micro-pressure waves, PK2201A2) of the Korea Railroad Research Institute.

References

- Adami, S. and H. J. Kaltenbach (2008). Sensitivity of the wave-steepening in railway tunnels with respect to the friction model. *In Proceedings of the BBAA VI International Colloquium on Bluff Bodies and Aerodynamic Applications*, Milano, Italy.
- Fukuda, T., S. Ozawa and M. Iida (2006). Distortion of compression wave propagating through very long tunnel with slab tracks. *JSME International Journal Series B* 4, 1156-1164.
- Hara, T. (1961). Aerodynamic force acting on a high speed train at tunnel entrance. *Bulletin of JSME* 4 (15), 547-553.
- Heine, D., K. Ehrenfried, G. Heine and S. Huntgeburth (2018). Experimental and theoretical study of the pressure wave generation in railway tunnels with vented tunnel portals. *Journal of Wind Engineering and Industrial Aerodynamics* 176, 290-300.
- Howe, M. S., M. Iida, T. Fukuda and T. Maeda (2000). Theoretical and experimental investigation of the compression wave generated by a train entering a tunnel with a flared portal. *Journal of Fluid Mechanics* 425, 111-132.
- Iida, M. and M. S. Howe (2007). Compression wave generated by a high-speed train entering a tunnel fitted with a hood with a long-slit window. *Journal of Low Frequency Noise, Vibration and Active Control* 26, 227-247.
- Iyer, R. S., D. H. Kim and H. D. Kim (2021). Propagation characteristics of compression wave in a high-speed railway tunnel. *Physics of Fluids* 33, 86-104.
- Iyer, R. S., D. H. Kim, T. H. Kim and H. D. Kim (2020). Effect of train speed on the formation process of entry compression waves generated by a high-speed train entering tunnel. In: *Recent Asian Research on Thermal and Fluid Sciences:*

- Proceedings of AJWTF7 2018*, Springer Singapore.
- Iyer, R. S., D. H. Kim and H. D. Kim (2018). Prediction of entry compression waves induced by a high-speed train entering tunnel. *Journal of Mechanical Science and Technology* 32, 5285-5292.
- Jun, K. J., Y. C. Hwang and C. Y. Yune (2017). Field measurement of temperature inside tunnel in winter in Gangwon, Korea. *Cold Regions Science and Technology* 143, 32-42.
- Kim, D. H., S. Y. Cheol, R. S. Iyer and H. D. Kim (2021). A newly designed entrance hood to reduce the micro-pressure wave emitted from the exit of high-speed railway tunnel. *Tunnelling and Underground Space Technology* 108, 103728.
- Kim, H. D. and T. Setoguchi (1999). Study of the discharge of weak shocks from an open end of a duct. *Journal of Sound and Vibration* 226, 23-29.
- Kozakevicius, A. J., D. Zeidan, A. A. Schmidt and S. Jakobsson (2018). Solving a mixture model of two-phase flow with velocity non-equilibrium using WENO wavelet methods. *International Journal of Numerical Methods for Heat and Fluid Flow* 28(9), 2052-2071.
- Li, Y. (2016). The effects of side branches on compression waves propagating in high-speed railway tunnels. *Advances in Structural Engineering* 16 (8), 1437-1446.
- Mashimo, S., E. Nakatsu and T. Aoki (1997). Attenuation and distortion of a compression wave propagating in a high-speed railway tunnel. *JSME International Journal Series B* 40 (1), 51-57.
- Matsuo, K., T. Aoki, T. Kashimura, H. Mashimo and S. Nakao (1996). Numerical study of attenuation and distortion of a compression wave propagating in a high-speed railway tunnel. *Transactions of Built Environment* 18, 1-10.
- Miyachi, T. (2017). Acoustic model of micro-pressure wave emission from a high-speed train tunnel. *Journal of Sound and Vibration* 391, 127-152.
- Miyachi, T., S. Ozawa, M. Iida, T. Fukuda and T. Arai (2016a). Propagation characteristics of tunnel compression waves with multiple peaks in the waveform of the pressure gradient: Part 2: theoretical and numerical analyses. *Proceedings of the IMechE Part F: Journal of Rail and Rapid Transit* 230 (4), 1309-1317.
- Miyachi, T., S. Saito, T. Fukuda, Y. Sakuma, S. Ozawa, T. Arai, S. Sakau and S. Nakamura (2016b). Propagation characteristics of tunnel compression waves with multiple peaks in the waveform of the pressure gradient: Part 1: field measurements and mathematical model. *Proceedings of the IMechE Part F: Journal of Rail and Rapid Transit* 230 (4), 1297-1308.
- Miyachi, T., T. Fukuda and M. Iida (2008). Distortion of compression wave propagating through Shinkansen tunnel. in: *Noise and Vibration Mitigation for Rail Transportation Systems: Proceedings of the 9th International Workshop on Railway Noise, Munich, Germany*, Springer Berlin Heidelberg.
- Mok, J. K. and J. Yoo (2001). Numerical study on high speed train and tunnel interaction. *Journal of Wind Engineering and Industrial Aerodynamics* 89, 17-29.
- Murray, P. R. and M. S. Howe (2010). Influence of hood geometry on the compression wave generated by a high-speed train. *Journal of Sound and Vibration* 329 (14), 2915-2927.
- Ouffa, S., D. Zeidan and D. Seba (2021). The WAF scheme for the isentropic drift-flux model of compressible two-phase flows. *Computers & Fluids* 229, 105091.
- Raghunathan, R. S., H. D. Kim and T. Setoguchi (2002). Aerodynamics of high-speed railway train. *Progress in Aerospace Sciences* 38, 1013-1052.
- Vardy, A. E. and J. M. B. Brown (1995). Transient, turbulent, smooth pipe friction. *Journal of Hydraulic Research* 33, 435-456.
- Vardy, A. E. and J. M. Brown (2000). Influence of ballast on wave steepening in tunnels. *Journal of Sound and Vibration* 238 (4), 595-615.
- Vardy, A. E., A. Bergant, S. He, C. Ariyaratne, T. Koppel, I. Annus, A. Tjsseling and Q. Hou (2009). Unsteady skin friction experimentation in a large diameter pipe. In *3rd IAHR International Workshop on Cavitation and Dynamic Problems in Hydraulic Machinery and Systems*, Brno, Czech Republic.
- Wang, H., B. Lei, H. Bi and T. Yu (2018). Wavefront evolution of compression waves propagating in high speed railway tunnels. *Journal of Sound and Vibration* 431, 105-121.
- Winslow, A., M. S. Howe and M. Iida (2005). Influence of a scarfed portal on the compression wave generated by a high-speed train entering a tunnel. *Journal of Low Frequency Noise, Vibration and Active Control* 24 (4), 203-217.
- Yamamoto, A. (1977). Micro-pressure wave radiated from tunnel exit (in Japanese). In *Spring Meeting of the Physical Society of Japan*, Japan.
- Zeidan, D., E. Romenski, A. Slaouti, E. F. Toro (2006). Numerical study of wave propagation in compressible two-phase flow. *International Journal of Numerical Methods for Heat and Fluid Flow* 54(4), 393-417.
- Zeidan, D., S. Govekar and M. Pandey (2021). Discontinuity wave interactions in generalized magnetogas dynamics. *Acta Astronautica* 180, 110-114.

Zhang, L., M. Yang, L. Zhi, X. Feng and J. Zhang (2017). Oblique tunnel portal effects on train and tunnel aerodynamics based on moving model tests. *Journal of Wind Engineering and Industrial Aerodynamics* 167, 128-139.

Zhao, P., J. Chen, Y. Luo, Y. Li, L. Chen, C. Wang and T. T. Hu (2020). Field measurement of air temperature in a cold region tunnel in north east China. *Cold Regions Science and Technology* 171, 102957.